Mutagenic Studies on Histidine 98 of Methylglyoxal Synthase: Effects on Mechanism and Conformational Change[†,‡]

Gregory T. Marks,[§] Majelle Susler,[§] and David H. T. Harrison*,[||]

Department of Biochemistry, Medical College of Wisconsin, 8701 Watertown Plank Road, Milwaukee, Wisconsin 53226-3548, and Department of Biochemistry and Molecular Biology, Rosalind Franklin University of Science and Medicine, North Chicago, Illinois 60064

Received October 10, 2003; Revised Manuscript Received January 21, 2004

ABSTRACT: Two detailed mechanisms [Marks et al. (2001) *Biochemistry 40*, 6805] have been proposed to explain the activity of methylglyoxal synthase (MGS), a homohexameric allosterically regulated enzyme that catalyzes the elimination of phosphate from DHAP to form enol pyruvaldehyde. This enol then tautomerizes to methylglyoxal in solution. In one of these mechanisms His 98 plays an obligate role in the transfer of a proton from the O_3 oxygen of DHAP to the O2 oxygen. To test this hypothesized mechanism, the variants H98N and H98Q were expressed and purified. Relative to the wild-type enzyme, the H98N variant shows a 50-fold decrease in k_{cat} with all other kinetic parameters (i.e., K_m, K_{PGA}, etc.) being nearly the same. By contrast, the *apparent* catalytic rate for the H98Q variant is 250-fold lower than that of the wild-type enzyme. Inorganic phosphate acts as a competitive inhibitor (with a K_i of 15 μM) rather than as an allosteric-type inhibitor as it does in the wild-type enzyme, and the competitive inhibitor phosphoglyolate (PGA) acts as an activator of this variant. These facts are explained by a shift in the conformational equilibrium toward an "inactive" state. When activation by PGA is accounted for, the catalytic rate for the "active" state of H98Q is estimated to be only 6-fold less than that of the wild-type enzyme, and thus His 98 is not essential for catalysis. Primary deuterium isotope effect data were measured for the wild-type enzyme and the two variants. At pH 7.0, the ^{D}V isotope effect (1.5) and the absence of a $^{D}(V/K)$ isotope effect for the wild-type enzyme suggest that the rate for the isotopically sensitive step is partially rate limiting but greater than the rate of substrate dissociation. Both the ^{D}V (2.0) and $^{D}(V/K)$ (3.4) isotope effects were more pronounced in the H98N variant, while the H98Q variant displayed an unusual inverse ^{D}V (0.8) isotope effect and a normal $^{D}(V/K)$ (1.5) isotope effect. The X-ray crystal structures of PGA bound to the H98Q and H98N variants were both determined to a resolution of 2.2 Å. These mutations had little effect on the overall structure. However, the pattern of hydrogen bonding in the active site suggests an explanation as to how in the wild-type and H98N mutated enzymes the "inactive to active" equilibrium lies toward the active state, while with the H98Q mutated enzyme the equilibrium lies toward the inactive state. Thus, the role of His 98 appears to be more as a regulator of the enzyme's conformation rather than as a critical contributor to the catalytic mechanism.

The enzyme methylglyoxal synthase (MGS,[1] EC 4.2.3.3) is a homohexameric protein that catalyzes an elimination reaction that converts dihydroxyacetone phosphate (DHAP) to form phosphate and the enol of methylglyoxal (pyruvaldehyde), which subsequently tautomerizes off the enzyme to form methylglyoxal. Traditionally, MGS is thought to be the first enzyme in the "methylglyoxal bypass of glycolysis", where DHAP is converted to methylglyoxal, followed by an internal disproportionation reaction catalyzed by glutathione, glyoxalase I, and glyoxalase II to form D-lactate (*1*). However, RNA expression profiling experiments show no significant correlation between the expression of *mgsA* and the expression of either *gloA* or *gloB* under a wide variety of conditions (Dr. Patrick Brown, Stanford University, personal communication). Thus, the physiological role for MGS in *Escherichia coli* is probably not that of glucose metabolism. *E. coli mgsA*$^{-}$ deletion mutants in the presence of cAMP express a slow growth phenotype, which is associated with difficulty in recovering from carbon starvation (*2*).

MGS kinetic data are either hyperbolic or sigmoidal with respect to substrate concentration in the absence or presence of phosphate, respectively (*3*, *4*). Thus, phosphate acts as an allosteric-type (conformational) inhibitor and not as a product inhibitor. For the wild-type enzyme in the presence of phosphate, there is cooperativity between active sites that occurs upon substrate binding. This is fundamentally different

[†] This research was supported by National Science Foundation Grant MCB-0213347 to D.H.T.H.

[‡] Coordinates have been deposited with the Protein Data Bank (PDB) (http://www.rcsb.org/pdb/:), ID codes 1S89 and 1S8A.

* To whom correspondence should be addressed at Rosalind Franklin University of Science and Medicine, 3333 Green Bay Road, North Chicago, IL 60064. E-mail: David.Harrison@finchcms.edu.

[§] Medical College of Wisconsin.

[||] Rosalind Franklin University of Science and Medicine.

[1] Abbreviations: MGS, methylglyoxal synthase; DHAP, dihydroxyacetone phosphate; GAP, glyceraldehyde 3-phosphate; PGH, phosphoglycolohydroxamic acid; PGA, phosphoglycolic acid; TIM, triosephosphate isomerase.

10.1021/bi035838o CCC: $27.50
Published on Web 03/11/2004

Scheme 1

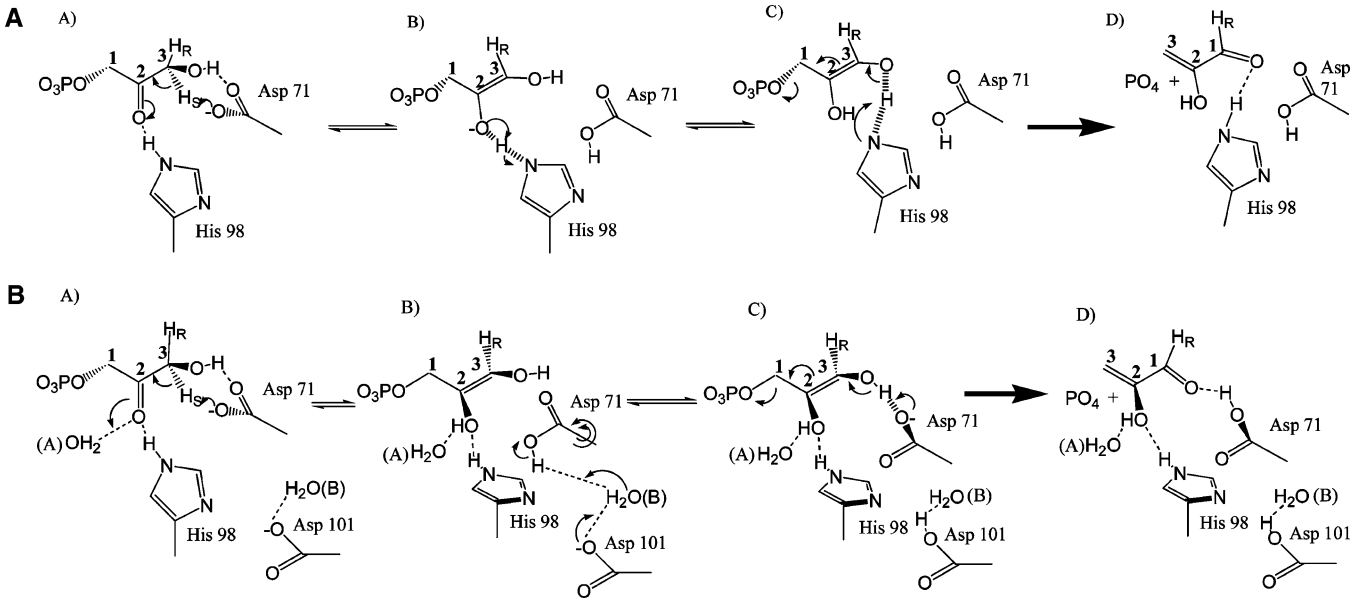

from the feedback control exerted on most allosterically regulated metabolic enzymes, which are typically effected by "downstream" products that bind at sites that are distinct from the active site (*5*). The three-dimensional structure of MGS shows that it is a hexameric enzyme and that there is no distinct site for phosphate to bind to the enzyme other than the phosphoryl binding site of the substrate and competitive inhibitors (*6*). The phosphate site overlaps the active sites and allows the substrate to compete with the allosteric-type inhibitor to relieve the conformational strain on the remaining protomers. It has previously been noted that phosphate inhibition is overcome by high quantities of substrate, so in this sense phosphate is a "competitive" inhibitor. It is unknown how many phosphate ions can bind a single hexamer in the "inactive" state or the binding constant for the phosphate ion. In the wild-type enzyme the binding to phosphate is necessary for the inactive state but not sufficient. There is crystallographic evidence that phosphate can also bind to an active site that is in all other respects in an "R-state" conformation (*6*). Thus, the equilibrium between the "active" and inactive states depends on the ability of the enzyme to distinguish a phosphate in the active site from a phosphoryl in the substrate or substrate analogue. The cooperative properties of hexameric MGS and its variants make interpretation of kinetic data somewhat more complex than that of a typical monomeric enzyme.

The initial steps catalyzed by MGS are reminiscent of the mechanism of triosephosphate isomerase (TIM) in that a catalytic base abstracts the C3 proton of DHAP to give rise to an enediolic intermediate (*7*). In TIM, Glu 165 abstracts the carbon proton with the assistance of His 95, which protonates the O2 oxygen and forms an unusual imidazolate anion. His 95 then abstracts a proton from the O3 oxygen of the enediol intermediate, and the C2 carbon is protonated by Glu 165 (*8*). The structure of methylglyoxal synthase bound to 2-phosphoglycolic acid suggested homologous roles for Asp 71 and His 98 to Glu 165 and His 95 from TIM, respectively (*9*). In Scheme 1A, a "TIM-like" mechanism is proposed where Asp 71 abstracts the C3 *pro-S* proton to form an enediolate intermediate. The negatively charged O2 oxygen abstracts the ϵ nitrogen of His 98 via a short, strong hydrogen bond to form an imidazolate anion. The imidazolate nitrogen can form a second short, strong hydrogen bond with the O3 hydroxyl group and abstract the hydroxyl proton. The enediolate then collapses in a 1,4-elimination reaction to form free inorganic phosphate and the enol of methylglyoxal. However, this TIM-like mechanism fails to explain the 10^2-fold difference in the binding constant for MGS binding to phosphoglycolohydroxamic acid (PGH) compared to that for TIM binding to PGH. Additionally, there is no role for the short, strong hydrogen bond that was found by both NMR spectroscopy and X-ray crystallography between the carboxylate of Asp 71 and the hydroxyl of PGH, and contrary to the prediction made by the TIM-like mechanism, there is a normal hydrogen bond to the ϵ nitrogen of His 98 (*10*). It also failed to explain previous MGS mutagenesis experiments, where D101N was shown to be $\sim 10^4$-fold down in activity compared to the wild-type enzyme activity (*4*). However, more recently, preliminary theoretical data suggest that Asp 101 may play an important role in the initial proton abstraction step that is common to both mechanisms (Qiang Cui, personal communication). These facts led to the proposal of an alternative "PGH-based" mechanism for catalysis by MGS shown in Scheme 1B. In the PGH-based mechanism, Asp 71 abstracts the *pro-S* proton to form the same enediolate intermediate that is ultimately protonated via a water molecule (H_2O A) by the surrounding bulk solvent. Asp 71 undergoes a conformational change in order to shuttle its proton via a buried water molecule (H_2O B) to Asp 101. A second conformational change then allows Asp 71 to form a short, strong hydrogen bond with the hydroxyl proton (similar to what is seen in the PGH complex). According to this scheme the initiation of the suprafacial 1,4-elimination of phosphate occurs when Asp 71 abstracts the hydroxyl proton of the enediolic intermediate.

To test the TIM-like mechanism, His 98 was mutated to either asparagine or glutamine. Asparagine and glutamine have the same hydrogen-bonding capacity as the δ or ϵ nitrogens of histidine, respectively, in both the protonated and unprotonated states. Here, we report the kinetic results

for these two mutated enzymes in the presence and absence of inhibitors. Additionally, we report both pH−rate profiles and kinetic isotope effects for the wild-type enzyme and the two variants. Lastly, we report the X-ray crystal structure of each of these mutated enzymes in the presence of the competitive inhibitor PGA. Combined, these studies suggest that His 98 is involved in the conformational mechanism of MGS "inactivation" and that the alternative PGH-based mechanism must contribute to the catalytic rate of the enzyme.

EXPERIMENTAL PROCEEDURES

Materials. Reduced glutathione, yeast glyoxalase I, aldolase from rabbit muscle, and the tris(monocyclohexylammonium) salt of phosphoglycolate (PGA) were purchased from Sigma Chemical Co. (St. Louis, MO). The pET16b-(+) bacterial expression vector was from Novagen (Madison, WI). DNA ligase and restriction enzymes were from Amersham Pharmacia Biotech (Piscataway, NJ). The YM-10 centrifugal filter concentrator was purchased from Millipore (Bedford, MA). All solvents and reagents were of analytical or reagent grade and were used without further purification unless otherwise indicated.

Construction of pMGS-H98N and pMGS-H98Q. Plasmids for expressing the two MGS variants were constructed by inserting DNA containing the mutated gene into the pET16b expression vector. The mutated genes were constructed by overlap extension PCR (*11*) using *Pfu* high-fidelity polymerase (with an annealing temperature of 58 °C) and the previously described pMGS plasmid (*4*) as a DNA template. The pMGS-H98N was constructed by generating two DNA fragments by PCR using the primer pairs (5′-CGGAATTCA***CTCGAG***TAAGAAACAGGTGGCGTTT-3′ and the mutagenic primer 5′-GCCGTGCCGAACGATCCTGACGTG-3′) and the primer pairs (the complement to the mutagenic primer 5′-CACGTCAGGATCGTTCGGCACGGC-3′ and 5′-GGAATT***CCATGG***AACTGACGACTCGCACTTT-3′). The DNA fragments were gel purified, mixed together, and thermocycled 30 times. The resultant 0.5 kb DNA fragment was gel purified, cut with the restriction endonucleases *Nco*I and *Xho*I, and ligated into a similarly restriction endonuclease treated pET16b expression vector. Construction of pMGS-H98Q followed the same method except that different mutagenic primers (5′-GCCGTGCCGCAGGATCCGGAC-GTG-3′ and 5′-CACGTCCGGATCCTGCGGCACGGC-3′) were used during the first PCR step. Sequences for the two mutated genes were determined (MCW protein and nucleic acid facility) to verify that only single base changes were made.

Expression and Purification of Wild-Type and Mutated MGS. Recombinant *E. coli* MGS was expressed from pET16-mgswt, pET16-H98N, or pET16-H98Q transformed ML1-(DE3) *E. coli* cells (an *mgsA*$^-$ strain, manuscript in preparation) and purified according to the method of Saadat and Harrison (*4*). These MGS proteins were found to be at least 95% pure as determined by 14% SDS−PAGE with Coomassie Blue staining and densitometric analysis as well as by the specific activity of the wild-type enzyme (1092 units/mg) using the assay described below.

Methylglyoxal Synthase Activity Assay. The glyoxalase I coupled assay of Hopper and Cooper (*3*) was used to determine the enzyme activity as described by Saadat and Harrison (*4*) at a constant temperature of 25 °C. Briefly, 0.7 mM DHAP in 50 mM imidazole (pH 7.0) is converted by MGS to produce methylglyoxal that forms a thiohemiacetal with glutathione (15 mM). The thiohemiacetal is isomerized by glyoxalase I (2 units) to form (*S*)-D-lactoylglutathione that absorbs light at 240 nm. The reaction was followed by monitoring the increased absorbance at 240 nm with a Shimadzu UV1650-PC spectrophotometer.

Protein Determination. Protein concentrations were determined by the Bradford dye binding assay (*12*) (Bio-Rad) using bovine serum albumin as the standard.

Enzyme Kinetics. Kinetic constants for the different variants of MGS were determined in the same manner as above although the concentration of DHAP was varied. For simple kinetics, each data point (initial velocity) was determined in at least duplicate and at least five different substrate concentrations. Control assays, lacking either substrate or enzyme, were routinely included and found to be negligible over the time course of the assay. Kinetic constants were calculated by fitting directly to the data with an unweighted least-squares analysis using the program GRAFIT (*13*). Steady-state kinetic data in the presence or absence of phosphate were fit to the Michaelis−Menten equation (eq 1) or the Hill-modified Michaelis−Menten equation (eq 2). Estimates of V for the active state of the H98Q enzyme were obtained by fitting the first phases of the more complex kinetics exhibited by this enzyme in the presence of PGA to a substrate inhibition model represented by eq 3, while a value for V/K of the active state of the H98Q enzyme was extrapolated from direct measures of V/K_{app} using eq 4. The acid and base pK_a's as well as the maximal catalytic efficiency for the pH−rate data were fit using eq 5. In these equations v_i is the observed velocity, V is the

$$v_i = VA/(K_m + A) \tag{1}$$

$$v_i = VA^h/(K_m + A^h) \qquad \text{where } S_{1/2} = K_m^{1/h} \tag{2}$$

$$v_i = \frac{V}{1 + K_m/A + A/K_{is}} \tag{3}$$

$$\frac{K_m'}{V} = \frac{K_m}{V} + \frac{[I]}{VK_I} \tag{4}$$

$$\frac{V}{K} = \frac{(V/K)_{max} \times 10^{pH-pK_{a1}}}{10^{2pH-pK_{a1}-pK_{a2}} + 10^{pH-pK_{a1}} - 1} \tag{5}$$

maximal velocity, A is the substrate concentration, h is the Hill coefficient, K_m is the Michaelis−Menten constant, K_m' is the apparent Michaelis−Menten constant, K_{is} is the substrate inhibition constant, $S_{1/2}$ is the substrate concentration when $v_i = V/2$, K_I is the competitive inhibition constant, pK_{a1} refers to the pK_a of the acidic limb of the pH−rate profile, and pK_{a2} refers to the pK_a of the basic limb of the pH−rate profile. The $(V/K)_{max}$ in eq 5 is the limit of optimal activity in V/K if the acidic residue was completely unprotonated at the same time as the basic residue was completely protonated.

Synthesis of DHAP. The dihydroxyacetone phosphate dimer was prepared according to the method of Jung et al.

(*14*) with adaptations by Pederson et al. (*15*) as described in the Supporting Information. DHAP was quantitated by an enzyme-coupled spectrophotometric assay (*16*).

Synthesis of d-DHAP and h-DHAP. DHAP in D_2O or H_2O was treated with aldolase for 1 h at room temperature to exchange the C3 *pro-S* proton of DHAP (*17*). The progress of the reaction was monitored by NMR spectroscopy. Controls were performed using DHAP in H_2O as well as DHAP in D_2O with no aldolase. The reaction mixture was spun through a Millipore YM-10 centrifugal filter concentrator to remove the aldolase. The amount of DHAP before and after treatment with aldolase was carefully quantitated, and losses were found to be minimal, on average 17%. Ultrafiltration was found to be superior to previously reported ion-exchange methods with regard to the overall yield of d-DHAP (*17*).

Phosphate Assay. The amount of phosphate contamination in the synthesized DHAP was measured using the method of Drueckes et al. (*18*) modified for larger volumes. Briefly, phosphate was combined with a solution of 15 mM zinc acetate and 10 mM ammonium molybdate at pH 5.0 and incubated at 30 °C for 5 min in 1 mL cuvettes. Color formation was compared to a standard curve of known phosphate concentrations at 630 nm. It was found that the aldolase-treated h-DHAP and d-DHAP typically had approximately twice the contaminating levels of phosphate than that of the untreated, with 8.5 mol % for an average untreated preparation and 15.4 mol % for an average treated preparation.

Crystallization and X-ray Data Collection of the H98N−PGA and H98Q−PGA Complexes. Orthorhombic crystals of H98N and H98Q MGS complexed with the competitive inhibitor PGA were grown using the hanging drop method against a solution containing 20% PEG 1500 and 100 mM sodium cacodylate at pH 6.2 and 6.0, respectively. Crystallization drops were made by mixing 4 μL of a 20 mg/mL MGS protein solution in 50 mM imidazole hydrochloride (pH 7.0), 1 mM KH_2PO_4, and 10 mM PGA with 4 μL of the well solution on a siliconized glass coverslip. The crystallization trays were incubated at room temperature for 1−2 weeks, in which time single hexagon prisms ranged in size between 100 μm and 1 mm in their largest dimension. Diffraction data were collected as previously described for wild-type MGS−PGA crystals (*9*). MGS crystals were mounted in sealed quartz capillaries, and data were collected using a Riguaku R-axis IIc image plate detector exposed to Cu Kα radiation focused and monochromated by Osmic elliptical optics and generated by a Rigaku RU-200 rotating anode X-ray generator with a 0.2 mm filament set to 50 kV and 100 mA. One degree rotation photographs were taken with a crystal to detector distance of 190 mm and a 2θ angle of 0°. Reduced diffraction data from five different crystals were combined in both cases, using the Program SCALEPACK from the HKL diffraction suite (*19*). The data collection statistics are presented in Table 1.

Refinement of the Mutant H98N and H98Q MGS−PGA Complex Structures. Prior to refinement, 7.5% of the data between 30.0 and 2.2 Å, selected in 15 discrete shells throughout the resolution range to avoid the biasing effects of noncrystallographic symmetry (NCS), was set aside for the calculation of the R_{free} factor (*20*) using the program DATAMAN (*21*). Using the structure of the previously determined wild-type MGS−PGA complex (*9*) without the PGA or water molecules included as a model for determining the initial phases, electron density maps were calculated by the program CNS (*22*) using $3F_o - 2F_c$ as Fourier coefficients. The electron density maps clearly revealed the presence and position of the bound PGA in each of the six active sites in the asymmetric unit. For H98N and H98Q, following the modeling of PGA and rigid body refinement, the *R*-factor was 28.8%/34.9% and the "free *R*-factor" (R_{free}) was 29.4%/25.8%, respectively. Following the addition of 148/101 water molecules, respectively, and several rounds of simulated annealing, positional refinement with noncrystallographic symmetry restraints, and five/six rounds of manual rebuilding using the program O (*23*), the *R*-factor converged to 19.0%/19.3% and R_{free} to 22.9%/22.8% for H98N and H98Q, respectively. The Ramachandran plot shows that 91.6%/93.3% of all residues fall within the most favored region. Refinement statistics are presented in Table 1.

Table 1: Crystal Parameters and Refinement Statistics

	H98N	H98Q
space group	$P2_12_12_1$	$P2_12_12_1$
cell dimensions (Å)	$a = 53.5$	$a = 53.1$
	$b = 129.5$	$b = 130.0$
	$c = 178.2$	$c = 178.8$
σ cutoff	0.0	0.0
resolution range (Å)	30.0−2.2 (2.24−2.20)[a]	30.0−2.2 (2.24−2.20)[a]
total no. of reflections	339560	523690
no. of unique reflections	60966	63824
no. of reflections used in refinement	50315 (1931)	57416 (2284)
completeness (%)	82.6 (65.0)	90.0 (72.5)
R_{symm} (%)	9.5 (23.3)	9.5 (29.0)
R_{free} (%)	22.9	22.8
R-factor (%)	19.0	19.3
Ramachandran most favored/additional (%)[b]	91.6/8.1	93.3/6.7
overall mean temperature factor (Å^2)	27.1	28.2
rmsd from ideal[c]		
bond lengths (Å)	0.006	0.007
bond angles (deg)	1.3	1.2

[a] Numbers in parentheses represent the last shell values. [b] Most favored and additional regions are as defined by PROCHECK (*37*). [c] Root-mean-square deviations are from Engh and Huber ideal values (*38*).

Structural Alignment. The program O (*23*) was used in a least-squares fitting algorithm to calculate a matrix that overlays one structure upon another for structural comparisons.

RESULTS

Kinetics of H98N and H98Q Variants of MGS. Freshly purified H98N and H98Q were used to determine the kinetic parameters using the spectrophotometric assay (*3*) described in Experimental Procedures. Both enzymes displayed decreased catalytic activity, and a summary of the kinetic constants determined can be found in Table 2. Paradoxically, the alteration of histidine 98 to asparagine has less of an effect on the observed kinetic constants than does the mechanistically more conservative change to glutamine (see Scheme 1). The H98N mutant behaved similarly to wild-type MGS in all respects other than the catalytic rate, k_{cat}

Table 2: Enzyme Kinetic Parameters

	k_{cat} (s^{-1})	K_m (mM)	k_{cat}/K_m (s^{-1}•mM^{-1})	K_{iPGA} (μM)	^{D}V	$^{D}(V/K)$
H98Q (−PGA)	0.96 ± 0.03	1.3 ± 0.2	0.7	ND[a]	0.78 ± 0.06	1.5 ± 0.3
H98Q (+PGA)	17−37[b]	0.6−1.2[b]	30.5	46−101[b]	<1	1.8
H98N	4.4 ± 0.4	0.26 ± 0.07	16.9	5.8 ± 0.8	2.00 ± 0.06[d]	3.4 ± 0.7[d]
wild type, pH 7.0	220 ± 10[c]	0.20 ± 0.03[c]	1100[c]	2.0 ± 0.4[c]	1.54 ± 0.05	1.0 ± 0.1
wild type, pH 6.0	179 ± 18	0.62 ± 0.15	289	ND[a]	1.5 ± 0.2	1.25 ± 0.11

[a] ND is not determined. [b] Estimates are based on PGA activation experiments; see Discussion for details. [c] From Saadat and Harrison (1998). [d] Hill coefficients of 1.8 ± 0.1 and 1.7 ± 0.1 were observed for these measurements for proteo- and deuterio-DHAP, respectively.

(4.4 ± 0.4 s^{-1}), which is decreased 50-fold, with a slightly elevated Michaelis constant, K_m (0.26 ± 0.07 mM). This corresponds to a $10^{1.8}$-fold decrease in k_{cat}/K_m versus the wild-type enzyme. Like the wild-type enzyme, the H98N variant shows cooperative behavior in the presence of phosphate (Figure 1A). When compared to the wild-type enzyme, the H98N variant is not as strongly inhibited by phosphate, although less phosphate is required to shift the kinetic plot from hyperbolic to sigmoidal. The enzyme exhibited sigmoidal character when using aldolase-treated (containing higher levels of contaminating phosphate; see Experimental Procedures) DHAP, whereas the wild-type enzyme did not. This effect was not measurable when using the untreated DHAP (containing lower amounts of contaminating phosphate; see Experimental Procedures).

The kinetic plot for the H98Q variant shows a slightly sigmoidal (Hill coefficient of 1.4) curve with a k_{cat} (0.96 ± 0.03 s^{-1}) that is nearly 250-fold lower than that of the wild-type enzyme and a K_m (1.3 ± 0.2 mM) that is nearly 6-fold larger than that of the wild-type enzyme. This corresponds to a $10^{3.2}$-fold decrease in k_{cat}/K_m compared to the wild-type enzyme. Additionally, phosphate acts as a competitive inhibitor for the H98Q variant with an inhibition constant, K_i, of 15 μM (Figure 1B). To understand the difference in kinetic behavior for these two highly related variants of His 98, it was necessary to examine the effects of a competitive inhibitor, PGA, on the kinetic behavior of these enzymes.

Inhibition by PGA on H98N and H98Q Variants of MGS. The structure of phosphoglycolic acid (PGA) is analogous to the enediolate intermediate and has been previously well characterized with both wild-type MGS (*4*) and TIM (*24*, *25*). The effects of varying the amount of PGA in the assay mixture on the kinetics of H98N and H98Q were determined. As expected, PGA behaved as a competitive inhibitor for the H98N variant with a K_i of 5.8 ± 0.8 μM. However, the kinetics of the H98Q enzyme behaved in an unusual manner in the presence of PGA. Consistent with the conformational equilibrium favoring the inactive state of the H98Q variant, the enzyme is activated with the addition of PGA to the assay mix (Figure 2A). With these data, however, we were unable to find a simple conformational model that could in its entirety adequately explain this set of curves (Figure 2B). Instead, the data shown in Figure 2B are fit to a substrate inhibition model for each different PGA concentration (see Supporting Information). Such a fit is not consistent with our understanding of the likely conformational mechanism of the H98Q enzyme; however, it does allow us to estimate the catalytic rate constant for the active enzyme. Using the initial slope of the velocity vs substrate curve (Figure 3, inset), k_{cat}/K_m can be determined by plotting $1/(k_{cat}/K_m)$ versus inhibitor concentration (Figure 3). At PGA concentrations greater than 50 μM, the value for k_{cat}/K_m was observed to decrease in a linear manner. Extension of this line back to the ordinate allows k_{cat}/K_m for the active state of the H98Q

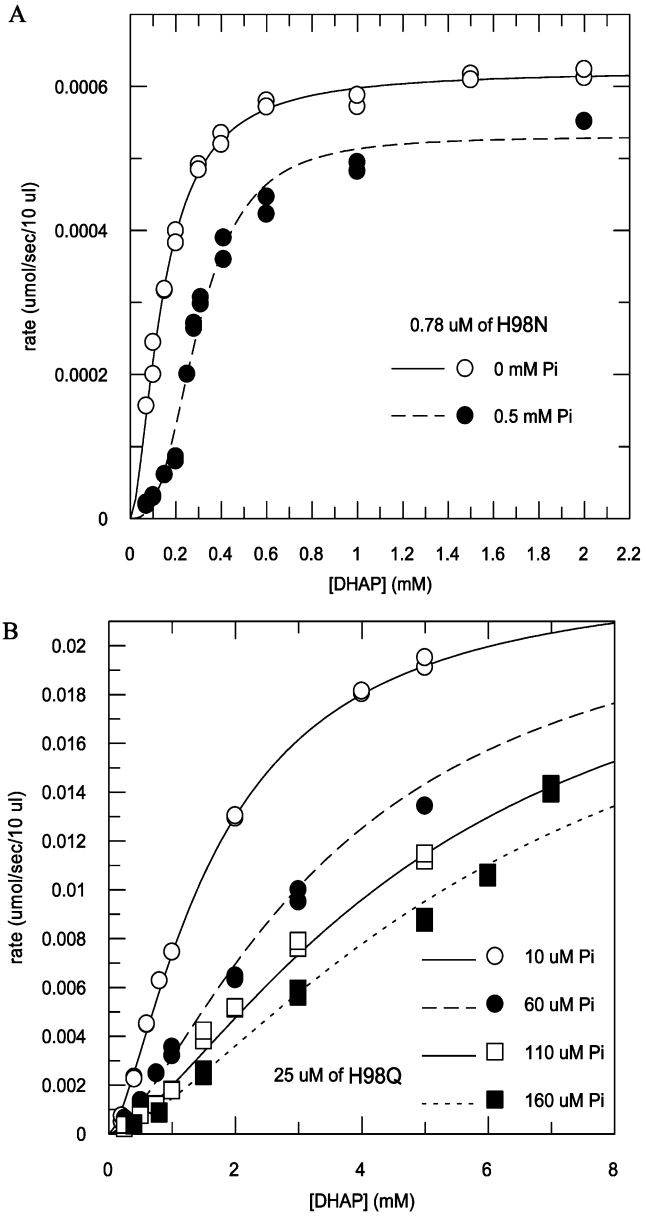

FIGURE 1: Effect of phosphate on the H98N and H98Q variants. (A) A plot of velocity versus substrate concentration in the absence and presence of 0.5 mM phosphate for the H98N variant. Note that the curve changes from hyperbolic to sigmoidal in shape. (B) A plot of velocity versus substrate concentration in the presence of 10, 60, 110, and 160 μM phosphate for the H98Q variant. The data fit a competitive inhibition model.

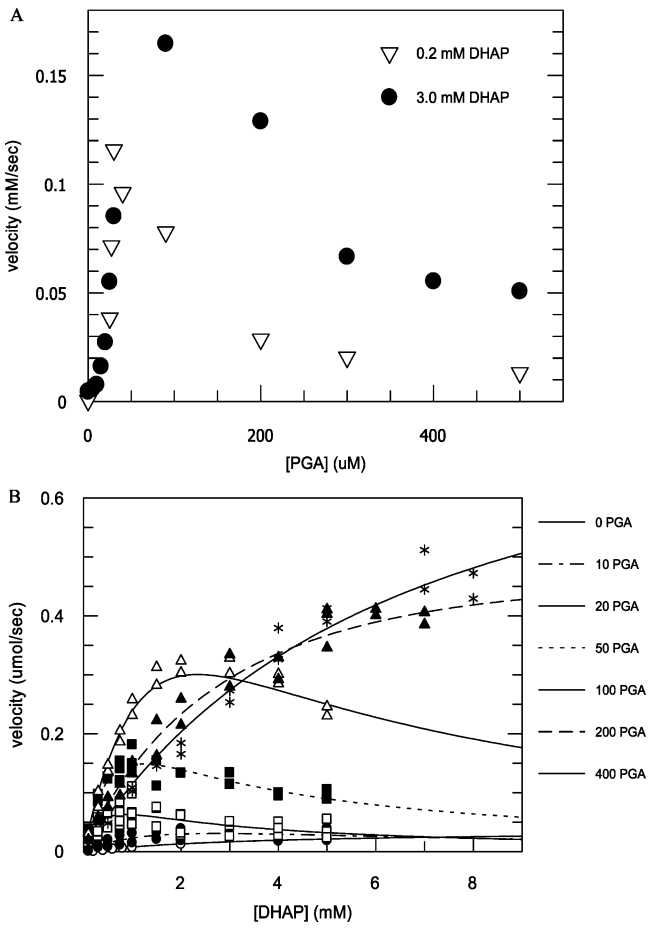

FIGURE 2: Activity of the H98Q variant as a function of DHAP and PGA concentration. (A) The activity at two fixed concentrations of DHAP is plotted against a varying amount of the competitive inhibitor PGA. This shows that PGA is acting as an activator, consistent with the H98Q variant resting in the T-state. (B) The activity of the H98Q variant at different fixed concentrations (μM) of PGA is plotted. Both the amount of DHAP required to reach maximal activity and the maximal activity of the H98Q variant are effected by the amount of PGA present. These curves are individually fit to a substrate inhibition model that does not explain the PGA effect.

mutated enzyme to be estimated at 30.5 mM^{-1} s^{-1}, 36-fold less than that of the wild-type enzyme. This estimate is likely to be low since more of the enzyme will be inactive at low concentrations of inhibitor than at high concentrations.

pH−Rate Profiles of H98N and H98Q. Wild-type MGS has previously been reported to have a pH optimum of 7.5 (*3*). This pH−rate profile is confirmed here, and it is compared to the pH−rate profiles of H98N and H98Q. The kinetic parameters from the hyperbolic fit to the data were used to determine the pH−rate profile of wild type and H98N. The linear portion of the velocity versus substrate concentration curve was used to estimate the k_{cat}/K_m for H98Q, where k_{cat} determinations were unreliable due to substrate limitations with high K_m values. The pH−rate profiles for both variants based on k_{cat}/K_m show optimal activity at more acidic pHs than that of the wild-type enzyme with the pH optima of 6.8 and 6.3 for H98N and H98Q, respectively. The H98N variant has a wider pH range of near-optimal activity than that of the wild-type enzyme, while the H98Q variant has a much narrower pH range of near-optimal activity than either of the other enzymes. The pH−rate profiles for the H98N and wild-type enzymes based on

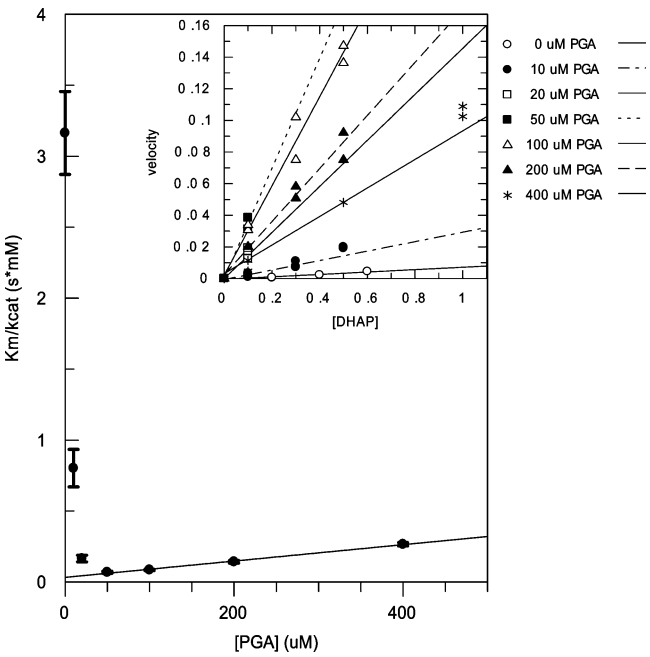

FIGURE 3: Determination of k_{cat}/K_m for H98Q. The initial slope of the velocity vs substrate curve from Figure 2B (inset), k_{cat}/K_m, was plotted as $1/(k_{cat}/K_m)$ versus inhibitor concentration. The extrapolation of the linear portion of the curve shows that the uninhibited H98Q R-state enzyme has a k_{cat}/K_m of 30.5 mM^{-1} s^{-1}.

Table 3: Enzyme pH Parameters

	pK_{a1}	pK_{a2}	pH optimum	k_{cat}/K_m limit
H98N	6.0 ± 0.1	7.6 ± 0.1	6.8	16 ± 2
H98Q	5.9 ± 0.2	6.7 ± 0.7	6.3	0.10 ± 0.03
wild type	6.9 ± 0.1	8.1 ± 0.1	7.5	1152.5 ± 159.4

	pK_{a1}	pK_{a2}	pH optimum	k_{cat} limit
H98N	5.5 ± 0.2	8.2 ± 0.2	6.8	2.88 ± 0.08
wild type	7.0 ± 0.1	7.9 ± 0.2	7.5	470 ± 80

k_{cat} show an even wider disparity in pK_{a1} for the two enzymes of 5.5 and 7.0, respectively. The individual pK_a's are presented in Table 3. It should be noted that eq 5 has two solutions, and the reduced chi-square was used to determine which solution is correct for wild type and H98N. In the case of H98Q the solutions are not as easily differentiated. While one solution is reported in Table 3, it is possible to invert the acidic and basic pK_a's for H98Q to give a solution of pK_{a1} equal to 7.0 ± 0.4, pK_{a2} equal to 5.6 ± 0.4, and a k_{cat}/K_m limit of 0.34 ± 0.26.

pH Effects on the Primary Deuterium Isotope Effect for Wild-Type MGS. Both h-DHAP and d-DHAP were made as described in Experimental Procedures and then used in the spectrophotometric assay. At pH 7.0 the ^{D}V and $^{D}(V/K)$ isotope effects are 1.5 and 1.0, respectively (Table 2). The $^{D}(V/K)$ isotope effect agrees with the tritium isotope effect, $^{T}(V/K)$, of 1.0 previously determined (*7*). When the pH of the assay buffer was lowered to 6.0, the ^{D}V isotope effect was unchanged but the $^{D}(V/K)$ isotope effect is elevated to 1.3. It is technically difficult to accurately measure deuterium isotope effects at lower pHs (unpublished results); however, it is clear that $^{D}(V/K)$ approaches ^{D}V when the pH is lowered.

Primary Deuterium Isotope Effects for H98N and H98Q. At pH 7.0, the ^{D}V isotope effect for H98N was found to be

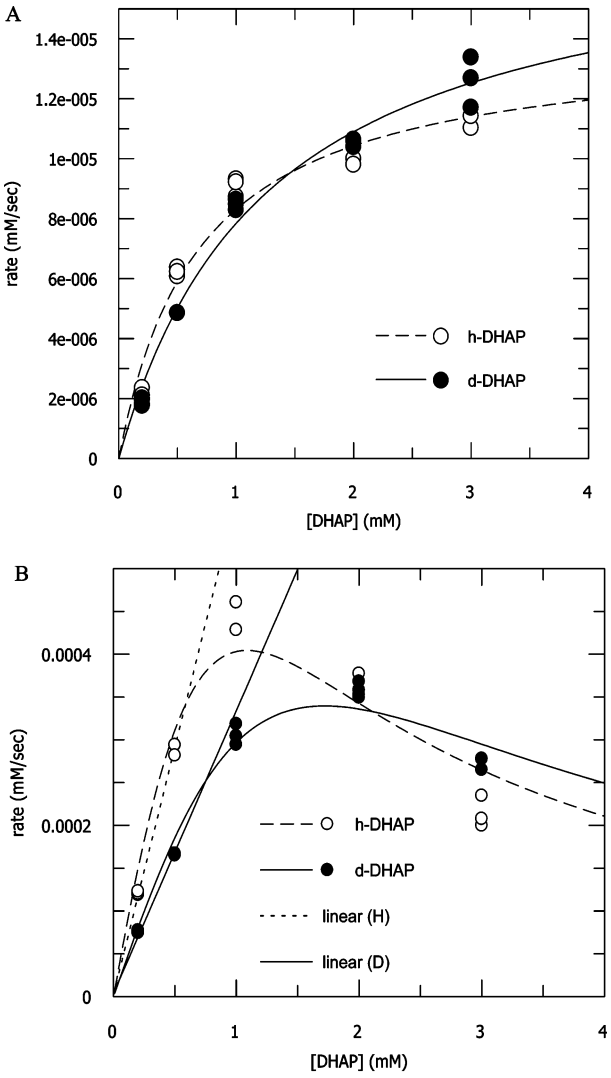

FIGURE 4: Primary isotope effects for H98Q. Plots of velocity versus substrate concentration show the effects of either proteo *pro-S* DHAP or deuterio *pro-S* DHAP in the absence (A) or presence (B) of 100 μM PGA. The dashed lines are fits to the data from h-DHAP, and the solid lines are fits to the data from d-DHAP. In the absence of PGA the $^{D}(V/K)$ isotope effect is 1.5, and in the presence of PGA the $^{D}(V/K)$ isotope effect is 1.8. Under both conditions an inverse ^{D}V isotope effect is observed.

2.0, slightly elevated from that for wild-type MGS; however, the $^{D}(V/K)$ was substantially elevated to 3.4 (Table 2). Again, H98Q behaved quite differently with a ^{D}V isotope effect of 0.8 and a $^{D}(V/K)$ isotope effect of 1.5 (Figure 4A). To verify the existence of the inverse ^{D}V isotope effect, the data were collected on two different occasions from two different mutant enzyme preparations. In each instance the calculated isotope effects and individual kinetic parameters upon which they were based were the same within the error of the measurement. Additionally, the H98Q variant in the presence of 100 μM PGA had a $^{D}(V/K)$ isotope effect of 1.8 (based on a linear fit to the first two data points) and an inverse ^{D}V isotope effect as judged the data at 3 mM DHAP (Figure 4B). The inverse ^{D}V isotope effect may be explained by the presence of a stronger critical "allosteric" hydrogen bond to the deuterium atom/ion during the course of catalysis. As such, d-DHAP might act like PGA and partially activate the H98Q variant (see the discussion below). To test this hypothesis, the deuterium isotope effect was measured for

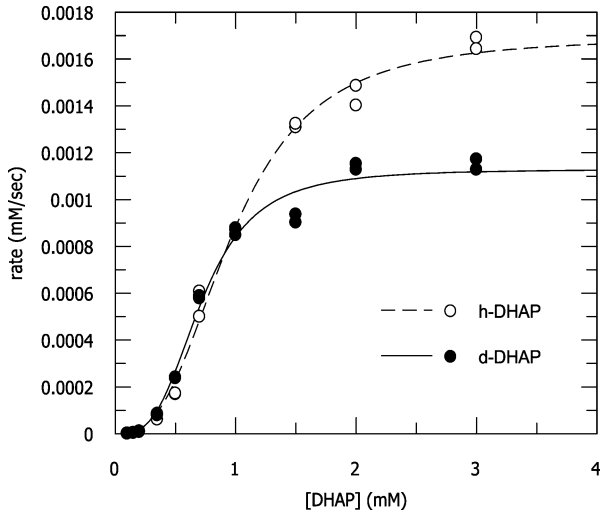

FIGURE 5: Primary isotope effect for the phosphate-induced T-state in wild-type MGS. The addition of 0.3 mM phosphate to wild-type MGS shifts its equilibrium toward the T-state. Under these conditions, the wild-type enzyme exhibits isotope effects of 1.5 and 0.6 for ^{D}V and $^{D}(V/K)$, respectively.

the wild-type enzyme in the presence of 0.3 mM phosphate (Figure 5). It was reasoned that at low substrate concentrations the phosphate-inhibited wild-type enzyme might behave similarly to that of the H98Q variant, since both enzymes are dominated by the inactive conformation. Indeed, the switch from the inactive to the active conformation happens at a lower concentration of d-DHAP than it does with h-DHAP as exemplified by a $^{D}(V/K)$ isotope effect of 0.6 for the wild-type enzyme in the presence of 0.3 mM phosphate. Since MGS bound to phosphate is in the inactive state, the inverse $^{D}(V/K)$ isotope effect simply indicates that the deuterated substrate shifts the equilibrium toward the active conformation more readily than does the protonated substrate. Saturating amounts of substrate drive the enzyme toward the active conformation, and thus the ^{D}V isotope effect (1.5) is identical to that of the enzyme in the absence of phosphate.

Structural Comparison of H98N−PGA and H98Q−PGA Complexes to the Wild-Type−PGA Complex. The X-ray structures of both variants complexed with PGA were determined to a resolution of 2.2 Å (Table 1). When compared to the wild-type crystal structure with PGA bound, as well as to each other, there are few changes in the structures of the variants (Figure 6). In both cases, each protomer is effectively identical to the other five protomers in the asymmetric unit with an average RMSD for α carbons of 0.21 Å for H98N and 0.17 Å for H98Q. Remarkably, the deviations decrease when like subunits are compared from the wild-type PGA structure to each of these new structures. The RMSD of the α carbons from an asymmetric unit from the wild-type PGA structure with that of the H98N PGA structure is 0.17 Å, while the comparison with the H98Q PGA structure is 0.13 Å. These deviations are within the error limits that are expected for two independent determinations of the identical crystal structures at this resolution.

In addition to the large-scale similarities, between the mutants and wild type, there is very little change to be found in the active site. The positions of the catalytically important Asp 71 and Asp 101 have changed less than 0.2 Å when the

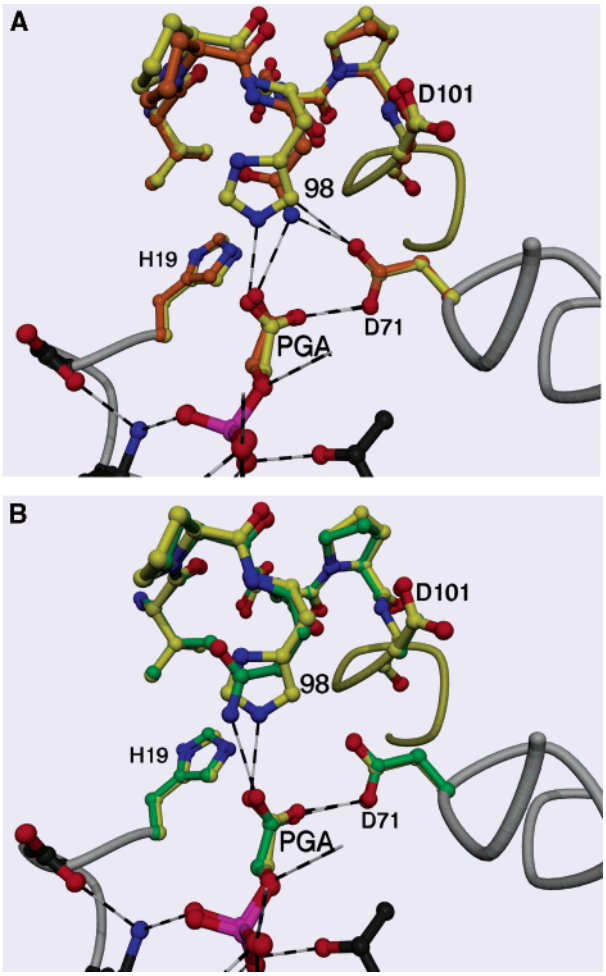

FIGURE 6: Comparison of the structures of H98N and H98Q to wild-type MGS. (A) The active site of H98N (orange) has been overlaid upon the active site of wild-type MGS (yellow), along with proposed hydrogen-bonding structure, with an RMSD of 0.17 Å. The distance between the aligned hydrogen bond donors, Asn Nδ and His Nϵ, is 1.3 Å, whereas the hydrogen bond distance has increased by 0.3 Å. (B) The active site of H98Q (green) has been overlaid upon the active site of wild-type MGS (yellow), along with proposed hydrogen-bonding structure, with an RMSD of 0.13 Å. The distance between the aligned hydrogen bond donors, Gln Nϵ and His Nϵ, is 1.0 Å, whereas the hydrogen bond distance has increased by 0.3 Å.

mutated and wild-type structures are superimposed. The largest change in the active site can be found around the position of the mutation. When the structure of the H98N variant is overlaid onto the structure of the wild-type enzyme, the relative position at the site of the mutation for the Cγ of the asparagine and the histidine residues differs by 0.6 $\pm$ 0.2 Å, while the hydrogen bond donor (Nδ of Asn or Nϵ of His) is displaced laterally by 1.3 $\pm$ 0.3 Å, although this change results in an elongation of the hydrogen bond from the protein donor to the PGA oxygen (O1) of only 0.3 Å (Table 4). When the structure of the H98Q variant is overlaid onto the structure of the wild-type enzyme, the relative position at the site of the mutation for the Cγ of the glutamine for five of the protomers and that of the histidine residues differ by 0.60 $\pm$ 0.06 Å. The glutamine for the remaining protomer is in a conformation that is not isomorphous to the histidine. In this case the relative distance for the Cγ is 1.1 Å. However, for all protomers there is a lateral displacement of 1.0 $\pm$ 0.3 Å at the Nϵ proton donor relative to the

Table 4: Atomic Distances from X-ray Crystal Structures

	distance (Å)
wild type	
PGA O2···Asp 71 Oδ2	2.78 $\pm$ 0.13
His 98 Cδ2···Asp 71 Oδ1	3.18 $\pm$ 0.04
His 98 Nϵ2···PGA O1	2.88 $\pm$ 0.02
His 98 Nϵ2···Asp 71 Oδ1	3.81 $\pm$ 0.04
H98N	
PGA O2···Asp 71 Oδ2	2.87 $\pm$ 0.13
Asn 98 Nδ2···Asp 71 Oδ1	2.89 $\pm$ 0.24
Asn 98 Nδ2···PGA O1	3.21 $\pm$ 0.17
H98Q	
PGA O2···Asp 71 Oδ2	2.84 $\pm$ 0.09
Gln 98 Nϵ2···Asp 71 Oδ1	4.93 $\pm$ 0.32
Gln 98 Nϵ2···PGA O1	3.24 $\pm$ 0.47

Scheme 2

A)

$$E^TP_i \qquad E^RPGA$$

$$K_{Pi} \uparrow\downarrow + P_i \qquad K_{PGA} \uparrow\downarrow + PGA$$

$$E^TS \underset{K_T}{\rightleftharpoons} E^T + S \underset{K_{eq}}{\rightleftharpoons} S + E^R \underset{K_R}{\rightleftharpoons} E^RS \xrightarrow{k_R} \text{Product}$$

$$K_{eq} = \frac{E^R}{E^T},\ K_T = \frac{[E^T][S]}{[E^TS]},\ K_R = \frac{[E^R][S]}{[E^RS]},\ K_{Pi} = \frac{[E^T][P_i]}{[E^TP_i]},\ \text{and}\ K_{PGA} = \frac{[E^R][PGA]}{[E^RPGA]}$$

Further, in the absence of any inhibitors,

$$v = \frac{V_{max}^{app}[S]}{K_m + [S]},\ \text{where}\ V_{max}^{app} = \frac{k_R E_0}{1 + \frac{K_R}{K_T K_{eq}}}\ \text{and}\ K_m = \frac{\frac{K_R}{K_{eq}} + K_R}{1 + \frac{K_R}{K_T K_{eq}}}$$

B)

$$E^T_6 \underset{K_1}{\rightleftharpoons} E^T_5E^R_1 \underset{K_2}{\rightleftharpoons} E^T_4E^R_2 \underset{K_3}{\rightleftharpoons} E^T_3E^R_3 \underset{K_4}{\rightleftharpoons} E^T_2E^R_4 \underset{K_5}{\rightleftharpoons} E^T_1E^R_5 \underset{K_6}{\rightleftharpoons} E^R_6$$

wild-type histidine that results in an elongation of the hydrogen bond to the PGA oxygen (O1) of only 0.3 Å. However, in the H98Q variant, there is no hydrogen bond from the glutamine nitrogen to the carboxyl of Asp 71, as can be found from the asparagine to Asp 71 in the H98N structure. These are the only significant observed structural differences.

DISCUSSION

Scheme 2 is presented as general model for understanding MGS kinetics and as a framework for further discussion. In Scheme 2A, we propose that the enzyme is in dynamic equilibrium between an active and an inactive conformation, both of which are competent to bind to the substrate, DHAP. This is in essence a "V-system" allosteric model with the distinguishing feature that the inactive conformation binds to phosphate much tighter than does the active form (for simplicity, we only show the binding to the inactive form). The other distinguishing feature of this model is that the active conformation binds to competitive inhibitors such as PGA much tighter than does the inactive conformation (again, for simplicity, we only show the binding to the active from). Thus, the wild-type enzyme can recognize the additional proton on a dianionic phosphate not found on a dianionic phosphoryl. From this scheme, it can be shown that, in the absence of inhibitors and when K_{eq} is large, both the apparent maximal velocity and Michaelis constant tend toward V_{max} and K_m for the active enzyme. Interestingly, it can also be shown that both the apparent V_{max} and K_m are affected by K_T and K_{eq}, when K_{eq} is small. Scheme 2B suggests that the conformational equilibrium of one protomer

in the hexamer is influenced by the conformations of its neighboring protomers. In the absence of these protein−protein interactions, both phosphate and PGA would appear to be competitive inhibitors. These interactions give rise to the sigmoidal-shaped kinetics sometimes observed for wild-type MGS and its variants.

Interpretation of H98Q Kinetics. The H98Q variant showed "normal" Michaelis−Menten kinetics with a k_{cat} that is nearly 250-fold less than that of the wild-type enzyme. Ordinarily, this fact might be interpreted as evidence supporting the TIM-like mechanism for MGS catalysis. However, the inhibition data lead to a different conclusion. In the wild-type enzyme, the presence of submillimolar concentrations of phosphate leads to sigmoidally shaped kinetic profiles that are increasingly "S-shaped" with increasing amounts of phosphate. The conformational equilibrium constant is thought to be much greater than 1 for the wild-type enzyme, and the binding of phosphate perturbs that equilibrium toward the inactive state (*1*). Kinetic studies of the H98Q variant show that phosphate acts as a competitive inhibitor, not as a conformational inhibitor (Figure 1B). The phosphate binding constant in the H98Q variant is of the same order of magnitude as the PGA binding constant for the wild-type enzyme; thus the binding site must be pre-organized to bind phosphate. This is the first indication that the "inactive to active" conformational equilibrium for the H98Q mutated enzyme favors the inactive state.

The kinetic profiles in the presence of PGA further support the idea that the H98Q variant is predominantly in the inactive state (Figure 2). However, there is not enough data for a stable fit of all parameters used in Scheme 2. Thus, estimates of k_{cat}, k_{cat}/K_m, and K_{PGA} for active state H98Q were obtained indirectly rather than from fitting these parameters to a single equation. At each concentration of PGA, the first phases of the individual kinetic profiles fit the substrate inhibition model (eq 3) very well (Figure 2B). Although there is a 2-fold variation in the value for V_{max} at PGA concentrations of 100, 200, and 400 μM (shown in Supporting Information), an upper limit on the catalytic rate constant for the active state of the H98Q variant can be derived from the catalytic rate determined by this substrate inhibition model at these competitive inhibitor concentrations, $k_{cat,upper} = 37\ s^{-1}$. A lower limit for the catalytic rate constant for the H98Q variant in the active state is simply the highest observed rate, $k_{cat,lower} = 17\ s^{-1}$. On the basis of these considerations we estimate the catalytic rate to be 10-fold lower than that of the wild-type enzyme.

By observing the initial slope at each concentration of PGA, k_{cat}/K_m' can be determined (Figure 3, inset). Equation 4 can then be used to extrapolate a value of k_{cat}/K_m for the R-state of the H98Q variant ($30.5\ mM^{-1}\ s^{-1}$). K_{PGA} can also be determined from the slope of the line and the estimated values for k_{cat}, $K_{PGA} = 75\ \mu$M. Thus, the H98Q mutated enzyme binds PGA about 10-fold less tightly than either the wild-type or the H98N mutated enzyme. For the H98Q variant, K_{PGA} can be regarded as the product of the equilibrium constant of PGA to the active enzyme and the conformational equilibrium constant for converting between the inactive and the active. In light of the crystal structure of the H98Q variant bound to PGA, where the number of hydrogen bonds to the PGA moiety is conserved relative to the wild-type and H98N mutated enzymes, the decrease in binding energy for PGA may be interpreted as a loss of a hydrogen bond in the H98Q variant as it goes from the inactive to the active state.

Scheme 3

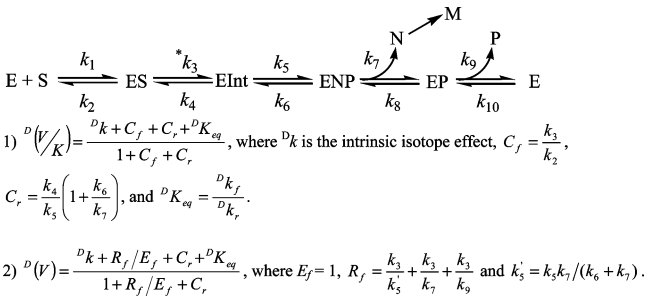

Interpretation of the Structure of the H98Q−PGA and H98N−PGA Complexes. It is strikingly apparent that, even near the site of the mutation, the structures of the H98Q−PGA and H98N−PGA complexes are virtually identical to the wild-type−PGA complex (Figure 6). This fact makes it clear that the structures of these variants are in the active conformation. Accordingly, the observed hydrogen-bonding patterns between the active site residues in these structures and the PGA molecule are similar with some minor changes in distances (Table 4). The PGA molecule does undergo some small conformational changes to make a hydrogen bond with the amide nitrogen of Asn 98 in this variant. This same conformational strain is likely to occur when DHAP binds to this variant. Additionally, there are significant changes in the angle of approach between the proton donor and the carboxylate oxygen of PGA. These subtle structural differences might explain the 10−50-fold decreases in k_{cat} for the mutated enzymes relative to the wild type.

The hydrogen-bonding pattern among the active site residues has changed in these variants. In the wild-type structure, the ϵ nitrogen of His 98 is pointed toward the carboxylate oxygen of PGA, and the δ carbon is in close proximity to the carboxylic oxygen of Asp 71 (3.2 Å). In the H98N variant, the δ nitrogen of Asn 98 donates a hydrogen bond to both the carboxylate oxygen of PGA and the carboxylic acid of Asp 71. In the H98Q variant, the ϵ nitrogen of Gln 98 is making a hydrogen bond to the carboxylate oxygen of PGA. Thus, the structures suggest that in the resting wild-type enzyme the imidazole ring of His 98 flips and the δ nitrogen makes a hydrogen bond to the carboxylate oxygen of Asp 71. When the substrate DHAP enters the active site, the imidazole ring is free to flip back to the PGA conformation and form a hydrogen bond between the ϵ nitrogen and the O2 oxygen of DHAP. Because Gln 98 of the H98Q variant is not able to form a hydrogen bond with Asp 71 due to steric constraints, the energetic balance between the active and the inactive state now favors the inactive.

Interpretation of Isotope Effect Data. In Scheme 3, the enzyme MGS (E) binds to the substrate DHAP, represented by S, with kinetic constants k_1 and k_2. The isotope-sensitive catalytic step converts the substrate to the enediolic intermediate, represented by Int, with kinetic constants k_3 and k_4. The intermediate is cleaved to form the products, the enol of pyruvaldehyde (N) and inorganic phosphate (P), with kinetic constants k_5 and k_6. The enol product comes off the enzyme with associated kinetic constants k_7 and k_8. Once

off the enzyme, the enol product tautomerizes to methylglyoxal (M). Lastly, phosphate leaves the enzyme with associated kinetic constants k_9 and k_{10}. The equations for the isotope effects $^{D}(V/K)$ and ^{D}V and the associated commitments to catalysis, C_f and C_r, were derived by Northrop (*26*), where ^{D}k is the intrinsic isotope effect and $^{D}K_{eq}$ is the change in the equilibrium constant due to the presence of the deuterium.

The isotope effects presented in Table 2 are explained in terms of Schemes 2 and 3. The wild-type enzyme is found to have a small but significant ^{D}V isotope effect and no measurable $^{D}(V/K)$ isotope effect at pH 7.0. This suggests that C_f, the forward commitment to catalysis, the ratio of k_{cat} (k_3) to k_{off} (k_2), must be large enough to completely mask the $^{D}(V/K)$ and the $^{T}(V/K)$ (*7*) isotope effect. Thus, for the wild-type enzyme, K_m for DHAP must be substantially larger than K_d. The relatively small value of the ^{D}V isotope effect suggests that some step other than the chemically sensitive step is partially rate limiting. The fact that $^{D}(V/K)$ approaches ^{D}V and that ^{D}V remains constant at pH 6.0 suggests that C_f is becoming smaller at lower pH (presumably by making k_2 larger).

The isotope effects measured for the H98N mutated enzyme show a slightly elevated ^{D}V and a greatly elevated $^{D}(V/K)$ isotope effect compared to the wild-type enzyme. Qualitatively, the "stickiness" of the substrate in this enzyme (C_f) is greatly reduced compared to the wild-type enzyme. The fact that ^{D}V is larger than that of the wild-type enzyme implies that the sum of C_r and R_f/E_f has decreased, which is consistent with the isotope-sensitive step, k_3, being decreased and the decreased "stickiness" of the substrate. Thus, His 98 plays a role in assisting C3 proton abstraction, yet the contribution that His 98 makes to k_5' must be reasonably small or the rate k_5' must be rather fast for the ^{D}V isotope effects to remain unmasked as a result of the change at this position. These data do not differentiate between the TIM-like and the PGH-based mechanisms.

The value of V_{max}(apparent) is sensitive to changes in K_R, while the value of K_m is insensitive to changes in K_R when the equilibrium constant is small (Scheme 2), as is the case in the H98Q enzyme. This is experimentally confirmed by the observed isotope effect for the phosphate-bound wild-type enzyme (Figure 5, discussed in Results). Thus, the inverse isotope effect seen on ^{D}V (0.8) is best explained by the deuterated substrate having a greater affinity for the active form of the enzyme than the protonated substrate and the observed isotope effect being reduced by a factor of approximately $[1 + (K_R^D/K_T K_{eq})]/[1 + (K_R^H/K_T K_{eq})]$ compared to the isotope effect that would be found for the active enzyme. Similarly, the observed $^{D}(V/K)$ isotope effect (1.5) is likely to be reduced by a factor of approximately (K_R^D/K_R^H) compared to that which would be found for the active enzyme. As would be expected from Scheme 2, when PGA is present (Figure 4B), the $^{D}(V/K)$ isotope effect increases to 1.8. This increase reflects the shift in the conformational equilibrium toward the active conformation. As with the enzyme in the absence of inhibitor, at high substrate concentrations the deuterated substrate yields a faster rate than the protonated substrate.

Interpretation of pH−Rate Profile Data. The pH−rate profiles for the mutated enzymes differ from that of the wild-type enzyme largely in the first pK_a (Table 3). In TIM, the acidic pK_a is associated with the ionization of the phosphoryl of DHAP (*27*). How the pK_a of the phosphoryl group of DHAP might be affected by this mutation is unclear, although the additional solvent volume afforded by the smaller asparagine residue might have an effect on the local dielectric constant. NMR titration studies have shown that His 98 is not protonated at pH 5.0 (*10*), suggesting that the removal of this residue cannot itself be responsible for the acidic pK_a in the pH−rate profile of the wild-type enzyme. If there are differences in the pK_a's of ionizable residues that control the two enzymes' respective rate-limiting step(s), then the observed change in the pH−rate profile can be accounted for by this change in the rate-limiting step(s) (this is likely the case for the H98Q enzyme). Alternatively, the entire mechanism in the wild-type enzyme might be different from that of the mutated enzyme [as was seen by the adoption of the "crisscross" mechanism in the H95Q variant of TIM (*28*)].

Relationship to Triosephosphate Isomerase Mutagenesis Studies. In TIM, the equivalent of the H98Q mutated MGS (H95Q) has been made and characterized by techniques of mechanistic enzymology (*28*). It is found that the H95Q mutated TIM has nearly 400-fold less activity than the wild-type enzyme. Further, on the basis of detailed isotope effect studies and the assumption that glutamine could not be acting as a proton donor, an alternative crisscross mechanism was proposed where glutamic acid 95 not only abstracts the C3 proton of DHAP but then places that proton on the O2 oxygen prior to abstracting the O3 proton prior to placing it on the C2 carbon. In some sense this mechanism is reminiscent of the PGH-based mechanism proposed for MGS in that the aspartic carboxylate abstracts not only the carbon proton but also the oxygen proton.

Under normal circumstances the substitution of glutamine for histidine would be considered a conservative substitution for the hydrogen-bonding character of the ϵ nitrogen of histidine without the possibility of proton transfer. However, theoretical calculations show that in TIM the catalytic histidine (His 95) is neutrally charged and donates its proton to the O2 oxygen to form a rare imidazolate anion (*8*, *29*). In both TIM and MGS, this possibility is verified experimentally by the observation of greatly lowered pK_a's for the catalytic histidinium cations (*10*, *30*). Thus, it is reasonable to assume that both enzymes proceed via a negatively charged imidazolate anion and that the small difference in the pK_a's of imidazole [the pK_a in water is 14.5 (*31*)] and acetamide [the pK_a in water is 15.1 (*32*)] becomes relevant to the interpretation of the histidine to glutamine variants for both enzymes. In TIM, the 400-fold loss of activity or the change in mechanism cannot be explained by the small difference in pK_a between a neutral histidine and glutamine in solution. Further, the tritium isotope exchange data support the crisscross mechanism and do not support the use of glutamine as a proton donor (*28*). Additionally, there is evidence that the crisscross mechanism occurs to a small extent in wild-type TIM by NMR and isotope exchange studies (*33*, *34*).

In the active state of H98Q MGS there is a much smaller loss in activity versus the wild-type enzyme than there is for the corresponding mutation for TIM; in fact, the difference in activity could be explained by the difference

in pK_a's for the two residues in solution. However, the activity of H98N MGS is only 50-fold lower than that of wild-type MGS rather than the 400-fold loss in activity for H98Q TIM. The crystal structure of the H98N variant shows that the "putative" hydrogen bond between Nδ2 of Asn 98 and the carboxylate oxygen of PGA has been extended over 0.3 Å relative to the wild-type Nϵ2 His 98 (Table 4). A further elongation of this distance would be expected for the substrate DHAP. Thus, the transfer of a proton from Nδ2 to the O2 oxygen of DHAP should be very inefficient. In TIM the deletion of a single methylene shortening the catalytic base has a 1000-fold effect on catalysis (*35*). Further, this asparagine amide proton is probably less acidic than the corresponding histidine proton due to the proximity of the aspartate 71 carboxylate oxygen. For these reasons we believe that the observed changes in k_{cat} are due to small changes in the way the substrate binds to the enzyme rather than the loss of histidine function.

What Advantage Might the PGH-Based Mechanism Confer on the Enzyme? Since the reaction catalyzed by MGS is thermodynamically favorable and the nonenzymatic kinetics favor elimination over isomerization for the substrate DHAP, it is difficult to hypothesize what catalytic advantage might be gained by utilizing a hydrogen from water rather than from histidine to protonate the O2 oxygen. Thus, it is possible that the adoption of the PGH-based mechanism by MGS is simply a consequence of building the active site within the microenvironment that is associated with the architecture of the $(\beta/\alpha)_5$-fold structural family. Unlike triosephosphate isomerase, methylglyoxal synthase must not only function efficiently but also be tightly regulated in order to give the bacteria an evolutionary advantage.

The PGH-based mechanism offers the appealing hypothesis that the equilibrium between the inactive and active states could be linked by the protonation state of Asp 101. The active conformation of MGS shows a salt bridge between Asp 101 on α-helix D of one protomer and Arg 107 on α-helix D of a second protomer in the hexamer (*6*). It is reasonable that this conformational signal disrupts this salt bridge. The disruption of the salt bridge brings the equilibrium constant between the active and inactive states closer to unity. Thus, during each catalytic cycle, the active site is capable of being switched into the inactive conformation by the binding of phosphate to an adjacent protomer. In other words, catalysis itself might be the grease that allows the binding of a single phosphate ion to disrupt the activity of the entire hexamer.

Conclusions. The kinetic data suggest that His 98 is not essential for catalysis, while the kinetic and structural data suggest that it is likely to play an important role in determining the equilibrium between the inactive and the active states. While this conclusion supports our previously adopted hypothesis that a PGH-based mechanism is an important contributor to catalysis, it does not address the importance of the TIM-like mechanism in the wild-type enzyme. The fact that the active states of the H98Q mutated enzyme and the H98N mutated enzyme are only reduced 10- and 50-fold, respectively, can be explained by subtle changes in substrate conformation within the context of the PGH-based mechanism. Since these data do not exclude the TIM-like mechanism from operating in the wild-type enzyme and there is no theoretical energy difference between the TIM-like and PGH-based mechanisms (*36*), we hypothesize that both the TIM-like mechanism and the PGH-based mechanism are available to wild-type MGS to convert the substrate to the product. Once Asp 71 has abstracted the C3 proton from DHAP, the O2 oxygen will be protonated either by His 98 or by water molecule A at rates that are nearly proportional to k_{cat} determined for the wild-type enzyme and H98Q, respectively. Once the O2 oxygen has been protonated, catalysis proceeds by the mechanism associated with the proton-donating group in a concerted or stepwise manner. This logic would suggest that the PGH-based mechanism operates as much as 20% of the time.

ACKNOWLEDGMENT

We thank Dr. June Brownlee of the University of Wisconsin at Milwaukee for critical discussions of the MGS mechanism, Dr. Paul Cook of University of Oklahoma for useful discussions regarding the allosteric effects displayed by the H98Q variant of *E. coli* MGS, and Dr. Dexter Northrop of the University of Wisconsin at Madison for critical comments. Additionally, we thank Dr. Valerie Grum-Tokars of the Chicago Medical School for providing valuable assistance in editing the final draft of the manuscript.

SUPPORTING INFORMATION AVAILABLE

Details of the synthesis of DHAP and a table of the individual parameters used to fit the data in Figure 2B. This material is available free of charge via the Internet at http://pubs.acs.org.

REFERENCES

1. Hopper, D. J., and Cooper, R. A. (1971) The Regulation of *Escherichia coli* Methylglyoxal Synthase; A new Control Site in Glycolysis?, *FEBS Lett. 13*, 213−216.
2. Tötemeyer, S., Booth, N. A., Nichols, W. W., Dunbar, B., and Booth, I. R. (1998) From famine to feast: the role of methylglyoxal production in *Escherichia coli*, *Mol. Microbiol. 27*, 553−562.
3. Hopper, D. J., and Cooper, R. A. (1972) The Purification and Properties of *Escherichia coli* Methylglyoxal Synthase, *Biochem. J. 128*, 321−329.
4. Saadat, D., and Harrison, D. H. T. (1998) Identification of Catalytic Bases in the Active Site of *Escherichia coli* Methylglyoxal Synthase: Cloning, Expression, and Functional Characterization of Conserved Aspartic Acid Residues, *Biochemistry 37*, 10074−10086.
5. Stryer, L. (1975) *Biochemistry*, W. H. Freeman, San Francisco, CA.
6. Saadat, D., and Harrison, D. H. T. (1999) The Crystal Structure of Methylglyoxal Synthase from *Escherichia coli*, *Struct. Folding Des. 7*, 309−317.
7. Summers, M. C., and Rose, I. A. (1977) Proton Transfer Reactions of Methylglyoxal Synthase, *J. Am. Chem. Soc. 99*, 4475−4478.
8. Bash, P. A., Field, M. J., Davenport, R. C., Petsko, G. A., Ringe, D., and Karplus, M. (1991) Computer simulation and analysis of the reaction pathway of triosephosphate isomerase, *Biochemistry 30*, 5826−5832.
9. Saadat, D., and Harrison, D. H. T. (2000) Mirroring Perfection: The Structure of Methylglyoxal Synthase Complexed with the Competitive inhibitor 2-Phosphoglycolate, *Biochemistry 39*, 2950−2960.
10. Marks, G. T., Harris, T. K., Massiah, M. A., Mildvan, A. S., and Harrison, D. H. T. (2001) Mechanistic Implications of Methylglyoxal Synthase Complexed with Phosphoglycolohydroxamic Acid as Observed by X-Ray Crystallography and NMR Spectroscopy, *Biochemistry 40*, 6805−6818.
11. Ho, S. N., Hunt, H. D., Horton, R. M., Pullen, J. K., and Pease, L. R. (1989) Site-directed mutagenesis by overlap extension using the polymersase chain reaction, *Gene 77*, 51−59.

12. Bradford, M. (1976) *Anal. Biochem. 72*, 248−254.
13. Leatherbarrow, R. J. (1994) GraFit: Data Analysis and Graphics Program [3.03], Erithacus Software Ltd.
14. Jung, S.-H., Jeong, J.-H., Miller, P., and Wong, C.-H. (1994) An Efficient Multigram-Scale Preparation of Dihydroxyacetone Phosphate, *J. Org. Chem. 59*, 7182−7184.
15. Pederson, R. L., and Wong, C.-H. (1991) An Improved Synthesis of Dihydroxyacetone Phosphate, *Tetrahedron 47*, 2643−2648.
16. Bergmeyer, H. U. (1984) *Methods in Enzymatic Analysis*, 3rd ed., Vol. II, pp 146−147, Verlag Chemie, Deerfield, FL.
17. Knowles, J. R., Leadlay, P. F., and Maister, S. G. (1972) Triosephosphate isomerase: isotope studies on the mechanistic pathway, *Cold Spring Harbor Symp. Quant. Biol. 36*, 157−164.
18. Drueckes, P., Schinzel, R., and Palm, D. (1995) Photometric Microtiter Assay of Inorganic Phosphate in the Presence of Acid-Labile Organic Phosphates, *Anal. Biochem. 230*, 173−177.
19. Otwinowski, Z., and Minor, W. (1996) *Book Title* (Carter, C., and Sweet, R. M., Eds.) pp 307−325, Academic Press, Boston, MA.
20. Brünger, A. T. (1992) The Free R Value: a Novel Statistical Quantity for Assessing the Accuracy of Crystal Structures, *Nature 355*, 472−474.
21. Kleywegt, G. J., and Jones, T. A. (1996) xdlMAPMAN and xdlDATAMAN—programs for reformatting, analysis and manipulation of biomacromolecular electron-density maps and reflection data sets, *Acta Crystallogr. D52*, 826−828.
22. Brünger, A. T., Adams, P. D., Clore, G. M., DeLano, W. L., Gros, P., Grosse-Kunstleve, R. W., Jiang, J.-S., Kuszewski, J., Nilges, M., Pannu, N. S., Read, R. J., Rice, L. M., Simonson, T., and Warren, G. L. (1998) Crystallography & NMR System: A New Software Suite for Macromolecular Structure Determination, *Acta Crystallogr. D54*, 905−921.
23. Jones, T. A., Zou, J. Y., Cowan, S. W., and Kjeldgaard, M. (1991) Improved methods for building protein models in electron density maps and the location of errors in these models, *Acta Crystallogr. A47*, 110−119.
24. Wolfenden, R. (1970) Binding of substrate and transition state analog to trisephosphate isomerase, *Biochemistry 9*, 3404−3407.
25. Lolis, E., and Petsko, G. A. (1990) Crystallographic analysis of the complex between triosephosphate isomerase and 2-phosphoglycolate at 2.5-Å resolution: implications for catalysis, *Biochemistry 29*, 6619−6625.
26. Northrop, D. B. (1982) Deuterium and tritium kinetic isotope effects on initial rates, *Methods Enzymol. 87*, 607−625.
27. Campbell, I. D., Jones, R. B., Kiener, P. A., and Waley, S. G. (1979) Enzyme-substrate and enzyme-inhibitor complexes of triose phosphate isomerase studied by 31P nuclear magnetic resonance, *Biochem. J. 179*, 607−621.
28. Nickbarg, E. B., Davenport, R. C., Petsko, G. A., and Knowles, J. R. (1988) Triosephosphate isomerase: removal of a putatively electrophilic histidine residue results in a subtle change in catalytic mechanism, *Biochemistry 27*, 5948−5960.
29. Cui, Q., and Karplus, M. (2001) Triosephosphate Isomerase: A Theoretical Comparison of Alternative Pathways, *J. Am. Chem. Soc. 123*, 2284−2290.
30. Lodi, P. J., and Knowles, J. R. (1991) Neutral imidazole is the electrophile in the reaction catalyzed by triosephosphate isomerase: structural origins and catalytic implications, *Biochemistry 30*, 6948−6956.
31. Walba, H., and Isensee, R. W. (1956) Spectroscopic Study of the Acid Strength of Imidazole, *J. Org. Chem. 21*, 702−704.
32. Borowell, F. G., and Algrim, D. (1976) Nitrogen Acids 1. Carboxamides and Sulfonamides, *J. Org. Chem. 41*, 2507−2508.
33. Harris, T. K., Abeygunawardana, C., and Mildvan, A. S. (1997) NMR studies of the role of hydrogen bonding in the mechanism of triosephosphate isomerase, *Biochemistry 36*, 14661−14675.
34. Harris, T. K., Cole, R. N., Comer, F. I., and Mildvan, A. S. (1998) Proton transfer in the mechanism of triosephosphate isomerase, *Biochemistry 37*, 16828−16838.
35. Raines, R. T., Sutton, E. L., Straus, D. R., Gilbert, W., and Knowles, J. R. (1986) Reaction energetics of a mutant triosephosphate isomerase in which the active-site glutamate has been changed to aspartate, *Biochemistry 25*, 7142−7154.
36. Zhang, X., Harrison, D. H., and Cui, Q. (2002) Functional specificities of methylglyoxal synthase and triosephosphate isomerase: a combined QM/MM analysis, *J. Am. Chem. Soc. 124*, 14871−14878.
37. Laskowski, R. A., MacArthur, M. W., Moss, D. S., and Thornton, J. M. (1993) PROCHECK: a program to check the stereochemical quality of protein structures, *J. Appl. Crystallogr. 26*, 548−558.
38. Engh, R. A., and Huber, R. (1998) Accurate bond and angle parameters for X-ray protein structure refinement, *Acta Crystallogr. A47*, 392−400.

BI035838O